Supplemental Information

Insights into the Nucleation and Growth of BiOCl Nanoparticles by *In Situ* X-ray Pair Distribution Function Analysis and *In Situ* Liquid Cell TEM

*Matthew N. Gordon,[a◊‡] Laura S. Junkers,[b‡] Jack S. Googasian,[a] Jette K. Mathiesen,[b†] Xun Zhan,[c§] David Gene Morgan,[c] Kirsten M. Ø. Jensen,[b] Sara E. Skrabalak[a]**

a Department of Chemistry, Indiana University, Bloomington, Indiana 47405, United States
b Department of Chemistry and Nanoscience Center, University of Copenhagen, 2100 Copenhagen Ø, Denmark
c Electron Microscopy Center, Indiana University, Bloomington, Indiana 47405, United States
‡ Contributed equally
◊ Present address: Savannah River National Laboratory, Aiken, SC 29808, United States
† Present Address: Surface Physics & Catalysis (SURFCAT), Department of Physics, Technical University of Denmark, 2800 Kgs Lyngby, Denmark
§ Present Address: Texas Materials Institute, University of Texas at Austin, Austin, Texas 78712, United States
*Corresponding Author Email: sskrabal@indiana.edu

Supplemental Information Table of Contents

Table of Contents 2

Supplemental Discussion of Background Subtraction Strategy 3

Supplemental Discussion of Side Product $Bi(C_2O_4)OH$ 3-4

Supplemental Discussion of Sequential Refinement Reliability 5

Movie Captions 6

Supplemental Figures 7-15

Supplemental Figure S1. Crystal structure of BiOCl 7
Supplemental Figure S2. LCTEM holder schematic 7
Supplemental Figure S3. STEM probe characterization 8
Supplemental Figure S4. Comparison of PDFs of applied backgrounds 8
Supplemental Figure S5. Refinements of BiClLac to the *ex situ* precursor PDF 9
Supplemental Figure S6. Refinement of BiClLac to the *in situ* precursor PDF 10
Supplemental Figure S7. Comparison of final F(Q) frame with the calculated reference patterns 10
Supplemental Figure S8. G(r) contour plot with an r_{max} of 30 Å 11
Supplemental Figure S9. F(Q) patterns overlaid with peaks assigned to the two product phases 12
Supplemental Figure S10. Crystal structure of $Bi(C_2O_4)OH$ 12
Supplemental Figure S11. PXRD data analysis of the product phase of two-step heating 13
Supplemental Figure S12. Refinement of BiClLac to the Figure 3a difference PDF 13
Supplemental Figure S13. Refinements of BiOCl to selected *in situ* PDF frames 14
Supplemental Figure S14. Complete sequential refinement results plotted against time 15

Supplemental Tables 15-23

Supplemental Table S1. xyz coordinates of atoms in the BiClLac complex 15-16
Supplemental Table S2. Results of refining BiClLac to the *ex situ* precursor PDF 17
Supplemental Table S3. xyz coordinates of atoms in BiClLac with refined Cl positions 18-19
Supplemental Table S4. Results of refining BiClLac to the *in situ* precursor PDF 19
Supplemental Table S5. Results of refining BiOCl to the *in situ* product PDF 20
Supplemental Table S6. Two-phase Rietveld refinement results of the product PXRD data 20
Supplemental Table S7. Results of refining BiOCl to the PDF corresponding to the PXRD data 21
Supplemental Table S8. Results of refining BiClLac to the Figure 3a difference PDF 21
Supplemental Table S9. Results of the initial step of the sequential refinement 22
Supplemental Table S10. Results of refining BiOCl to selected *in situ* PDFs between 40-55 min 22
Supplemental Table S11. Results of refining BiOCl to selected *in situ* PDFs between 60-75 min 23

Supplemental References 23

Supplemental Discussion of Background Subtraction Strategy:

The intense peak at 0.75 Å occurring in the experimental precursor PDF (Figure 1b) led us to further assess the background subtraction strategy. Figure S4 compares how two approaches of background subtraction affect the resulting PDF of the BiClLac precursor. The 'combined background' subtraction scales the combined scattering contributions of the ClLac solution and the NMR tube together, whereas the 'separate background' scales the two separately. The resulting PDFs shown in Figure S4a mainly differ in the relative intensity of the peaks between 0.75 Å and *ca*. 2.45 Å. Since the distance of 0.75 Å is too short to be assigned to an interatomic bond, it likely originates in mathematical artefacts from the Fourier transform[1] or the subtractions of the background instead.

To exclude the latter, the 'separate background' subtraction was used to minimize the peak at 0.75 Å without oversubtracting the Si-O distance *ca*. 1.6 Å[2]. Such separate scaling can account for slight variations in experimental parameters like the NMR tube thickness and the concentration of ClLac between measurements. Even this more careful treatment of the background did not, however, allow us to fully get rid of the artefact. A comparison of all background PDFs with that of the precursor solution prior to background treatment is given in Figure S4b and c. This comparison reveals that the 0.75 Å peak is more pronounced in the data obtained from solutions than in that of the empty NMR tube. The precursor solution PDF furthermore exhibits a more pronounced 0.75 Å peak than the ClLac background. Since the origin of this intense peak at low r has not been conclusively identified, the structural insight obtained from the respective PDFs must be handled with caution. Nevertheless, both applied background subtractions exhibit the same key features which highlight the robustness of certain structural features across different background treatments. Furthermore, the lack of an automated approach to apply the 'separate background' treatment to each frame made the 'separate' approach time-prohibitive. The background treatment of data discussed in the main text is accordingly limited to the 'combined background' approach.

Supplemental Discussion of Side Product $Bi(C_2O_4)OH$:

As highlighted in Figures S7 and S9, the F(Q) data acquired during BiOCl synthesis showed the formation of the side product $Bi(C_2O_4)OH$. This phase was, however, not apparent in the real space data (Figures 2b and 2e). To gain further insight, its presence was therefore investigated in reciprocal space.

The high Q range covered by TS data acquired with the RA-PDF setup[3] is generally paid for in a lower Q resolution. Therefore, additional PXRD data, *i.e*., data acquired with a longer sample-to-detector distance than the TS data frames, of the reaction product was collected at room temperature. Everything but the sample-to-detector distance and the temperature remained the same. Figure S11 shows this PXRD data. Note that the PXRD measurement was conducted after a BiOCl synthesis other than the one shown in Figure 2. The Figure S11 product formed after first heating to 70 °C and then increasing the temperature to 90 °C. The absolute structural parameters might therefore differ from the data shown throughout the rest of the paper. Nevertheless, this data set is suitable for identifying the nature of the side product, which has been found before in the F(Q) frames in Figures 2, S7, and S9.

Inspecting the 2D PXRD diffraction pattern and its calibrated form (Figure S11a), makes clear, that both solid diffraction rings and spotty ones are present. This difference between the rings indicates that two products are formed. One of them complies with the requirement of powder diffraction of a statistically random orientation of numerous small particles to generate solid rings, while the other one is apparently comprised of fewer grains of larger size.[4] This generates several distinct diffraction spots instead of continuous diffraction rings. As a comparison of both the 2D PXRD data with the *hkl* positions of BiOCl and $Bi(C_2O_4)OH$ shows, the solid diffraction rings can clearly be attributed to BiOCl.[5] The diffraction spots, on the other hand, match a reference pattern for bismuth oxalate hydroxide, $Bi(C_2O_4)OH$.[6]

A two-phase Rietveld refinement of these two phases to the 1D respective PXRD data is shown in Figure S11b as well. Due to the lack of PXRD data from the empty NMR set-up, a polynomial was used to fit the background. Accordingly, the background corrected R_{wp} value, resulting in 18.7 %, was used. When focusing on the difference curve, it becomes apparent that an overall reasonably good fit is obtained. The main mismatches between data and model occur at Bragg peak positions of $Bi(C_2O_4)OH$, *e.g.*, its (020) peak at 1.22 $Å^{-1}$. As can be seen in the difference curve, both the intensity and peak shape of this Bragg peak have not been properly modelled. Similar mismatches can be seen between 2.0 and 2.5 $Å^{-1}$, where several $Bi(C_2O_4)OH$ peaks overlap with BiOCl ones. These limitations in modelling the $Bi(C_2O_4)OH$ contributions of the XRD pattern are likely rooted in the spottiness of the $Bi(C_2O_4)OH$ diffraction rings. The presence of only a few, larger grains, as for $Bi(C_2O_4)OH$, cause a lack of statistics, when it comes to which of the crystallites' lattice planes meet the Bragg condition. This results in the diffracted intensity being unevenly distributed both within individual rings and between rings. Since the spots are integrated radially to obtain 1D diffraction patterns, it impacts the intensity, whether an arbitrary number of individual Bragg spots is integrated over or a full Debye-Scherer ring. Accordingly, the intensities of the $Bi(C_2O_4)OH$ Bragg peaks in the 1D pattern shown in Figure S11 are somewhat unreliable.

Intensity deviations in scattering data have a direct influence on the respective PDFs. As the PDF is the result of a Fourier transform of numerous Bragg peaks over a wide angle range, this influence cannot be easily defined. It is certain, that the presence of the $Bi(C_2O_4)OH$ side phase has an impact on the product PDFs. Based on the difference curves observed in Figures S11c and 3b, however, no structural information on the side product can be extracted from those PDFs.

Analogously to the fit in Figure 3b, both the Rietveld refinement and the real space refinement of the respective PDF in Figure S11c indicates a widened interlayer spacing of the formed BiOCl product (c = 7.4637 Å and c = 7.4933 Å, respectively). These results show the variability of the exact c parameter while highlighting the reproducibility of the widened gap between layers of BiOCl particles formed in solution.

Using PXRD data complementarily to the TS data, the side phase was identified. The origin of the observed $Bi(C_2O_4)OH$ formation is discussed in the main text.

Supplemental Discussion of Sequential Refinement Reliability:

As shown in Figure 4d and even more pronounced in Figure S14d, the fit agreement parameter R_w of the sequential PDF refinement approaches 1 towards the beginning of the experiment, *i.e.,* shorter heating times. This indicator for insufficient fit quality is in line with the absence of BiOCl (ICSD code 74502)[5] crystallites in the unheated solution. Nevertheless, the lack of fit quality at shorter heating times requires us to exclude parts of the sequential refinement from the subsequent interpretation. Only refinements, where the BiOCl model is visibly refined to features matching a BiOCl PDF pattern will yield reliable refinement results. Assessing which time span of the experiment was fitted well enough to be trusted for further interpretation is therefore of great importance.

To determine the reliable time span of the sequential refinement, we selected frames between 40 and 75 min, separated by 5 min time steps, for individual PDF refinements. Their results are shown in Figure S13. The refinements were conducted without Nyquist data sampling but are, apart from that, equivalent to their sequential counterpart.

Since the R_w value alone is not sufficient for determining the reliability of a refinement, the cut-off time used in Figure 4 was chosen based on the visual comparison given in Figure S13. The figure clearly shows how the BiOCl model becomes a more suitable description of the experimental PDFs upon prolonged heating time. The noise level in the frame acquired after 40 min heating exceeds, for instance, the intensity of possible BiOCl peaks in this PDF. Similarly, the PDFs obtained after 45 and 50 min of heating might contain BiOCl contributions, but of too low intensity to be reliably distinguished from noise or BiClLac contributions. This changes from 55 min of heating onwards. Although the 55 min refinement still has an exceedingly high R_w value of 0.715, PDF peaks characteristic for BiOCl are clearly visible up until *ca.* 23 Å. This facilitates a reliable refinement of the lattice parameters. Accordingly, the time span covered in Figure 4 was chosen from 55 min of heating to the final frame of the experiment (76.6 min of heating).

Movie Captions:

Movie 1. TEM movie of BiClLac precursor being heated causing BiOCl formation and growth. Particle formation begins at 06:14 forming nanoplates. Particles diffuse at elevated temperatures forming aggregates. *Conditions:* Field of view is 9.42 μm x 9.42 μm (4096 x 4096 pixels). Sample is heated at 5 °C/min from room temperature. The lower banner displays time in minutes:seconds (mm:ss) (left), current temperature in °C (middle) and scale bar (right). Total experiment time 09:00, recorded at 5 fps (2700 frames total). Every 8th frame is played for the first 6:00 at 25 fps (40x actual speed). From 6:00–9:00, every frame is played at 25 fps (5x actual speed). Dose rate is 0.29 $\frac{e^-}{Å^2 * s}$.

Movie 2. Higher magnification STEM movie of BiClLac precursor being heated causing BiOCl formation and growth with single particle tracking. At left is the cropped and stabilized STEM movie following a particle(s). At right is a plot of 2D particle area (nm^2) vs time. The plot is animated as the particle is measured in each frame. The black area in the last frame is where the particles drifted near the edge of the field of view and was applied during drift correction. *Conditions:* Samples are heated at 3 °C/min from room temperature at 00:00. The lower banner displays time in mm:ss (left), current temperature in °C (middle) and scale bar (right). Full image processing steps for this movie can be found in Movie S1. Selected frames from this movie can be found in Figure 7.

Movie S1. Higher magnification STEM movie of BiClLac precursor being heated causing BiOCl formation and growth with single particle tracking and detailing the data processing steps sequentially. The first part of the movie plays the raw STEM movie (00:00 – 09:55), followed by the cropped and stabilized STEM movie following three particles: left, middle, and right. At right is a plot of particle area (nm^2) vs time. The plot is animated as the particle is measured in each frame. The next portion of the video shows the particle thresholding based on the Triangle algorithm[7] (white particle on black background), followed by the particle size measurements outlined in blue (black particle on a white background). *Conditions:* Field of view in raw movie is 280 nm x 280 nm (1024 x 1024 pixels). Probe current was 0.097 nA with a dwell time of 3.81 μs/pixel using spot size M. Probe size and distribution is shown in Figure S3. Sample is heated at 3 °C/min from room temperature at 00:00. The lower banner displays time in mm:ss (left), current temperature in °C (middle) and scale bar (right). Total experiment time 09:55, recorded at 1 frame every 5.6 s (107 frames total), and played at 3 fps (16.8x actual speed).

Movie S2. STEM movie of BiClLac precursor under electron beam radiation without heating as a control experiment. Sample is kept at 22 °C from 00:00 to 44:34. No particle formation or growth occurs. After this, heating is activated. Particle formation then begins at 57:36, showing that the reaction is triggered by heat and not the electron beam alone. *Conditions:* Field of view is 1024 x 1024 pixels and 13.46 μm x 13.46 μm. Probe current was 0.29 nA with a dwell time of 8 μs/pixel using spot size L. Probe size and distribution is shown in Figure S3. Applied sample heating begins starting at 44:34 at 3 °C/min from room temperature to 60 °C and then held at 60 °C for the rest of the experiment. The lower banner displays time in mm:ss (left), current temperature in °C (middle) and scale bar (right). Heating begins at time 44:34 and reaches 60 °C at 57:16. Total experiment time 65:40, recorded at 1 frame every 9.9 s (400 frames total), and played at 5 fps (49.5x actual speed).

Supplemental Figures:

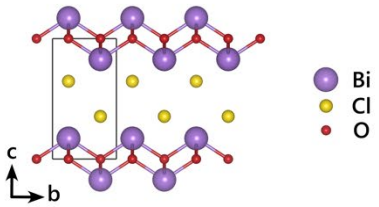

Figure S1. Crystal structure of BiOCl (ICSD code 74502)[5] shown along the *a* axis. Bi, Cl, and O atoms are visualized in purple, yellow, and red, respectively.

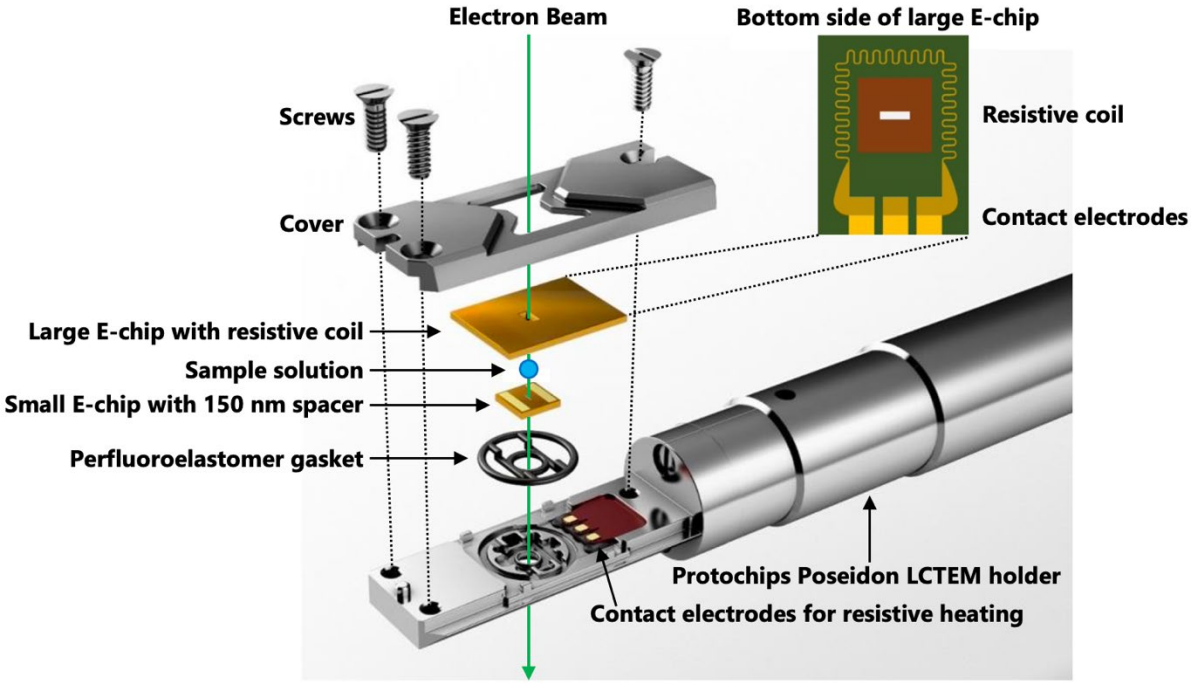

Figure S2. Exploded view of the assembled LCTEM holder used in the experiments. Original images courtesy of Protochips, Inc. (2020).

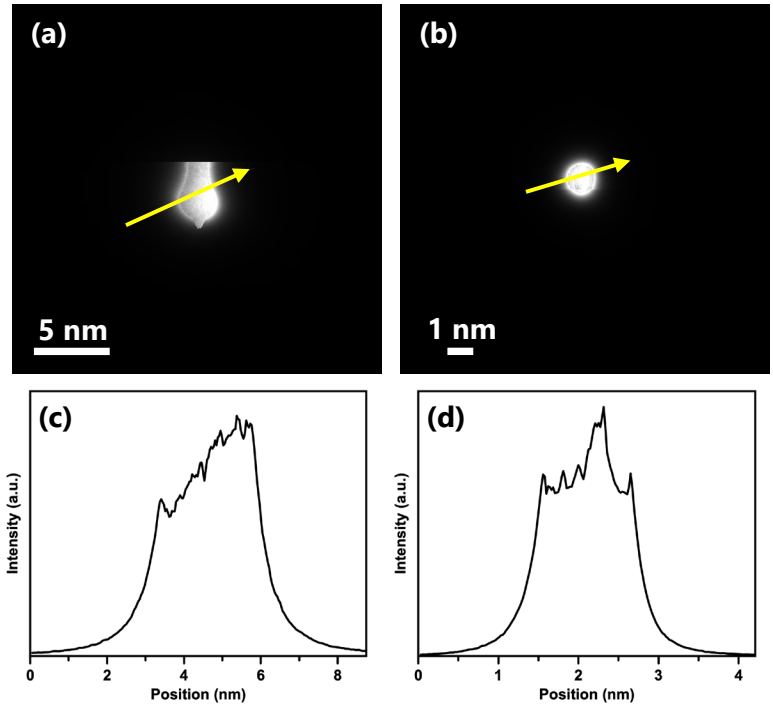

Figure S3. Images of the STEM probe (a,b) and intensity line scans along the yellow lines (c,d) for spot sizes L (a,c) and M (b,d) as a measure of electron distribution in STEM mode. Exposure time was 0.05 s.

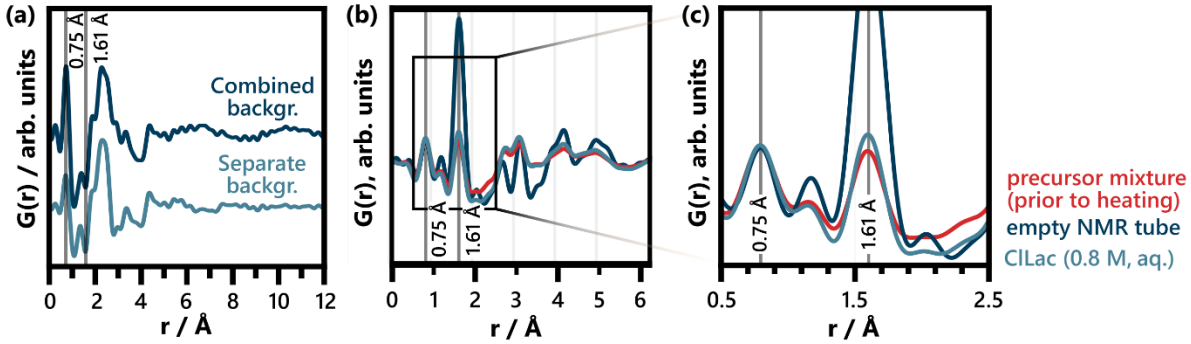

Figure S4. (a) Comparison of PDFs of the precursor solution based on two different background subtraction approaches. 'Combined background' refers to using one common background of 0.8 M ClLac solution in the *in situ* setup and is the background one used throughout the main text. 'Separate background' refers to using separate scaling factors for the glass contribution of the NMR tube setup and the ClLac solution. (b) Comparison of PDFs of possible backgrounds with the PDF obtained from the precursor solution without any background subtraction. All the shown PDFs were obtained based on a common composition estimate of $Bi(C_3H_4O_3Cl)_3(C_3H_5O_3Cl)$. 'ClLac (0.8 M, aq.)' refers to the ClLac solution background measured in an NMR tube (c) Zoom into plot (b) in the region of interest between 0.5 and 2.5 Å. The unphysical peak at 0.75 as well as the Si-O distance at 1.16 are highlighted for facilitated comparability.

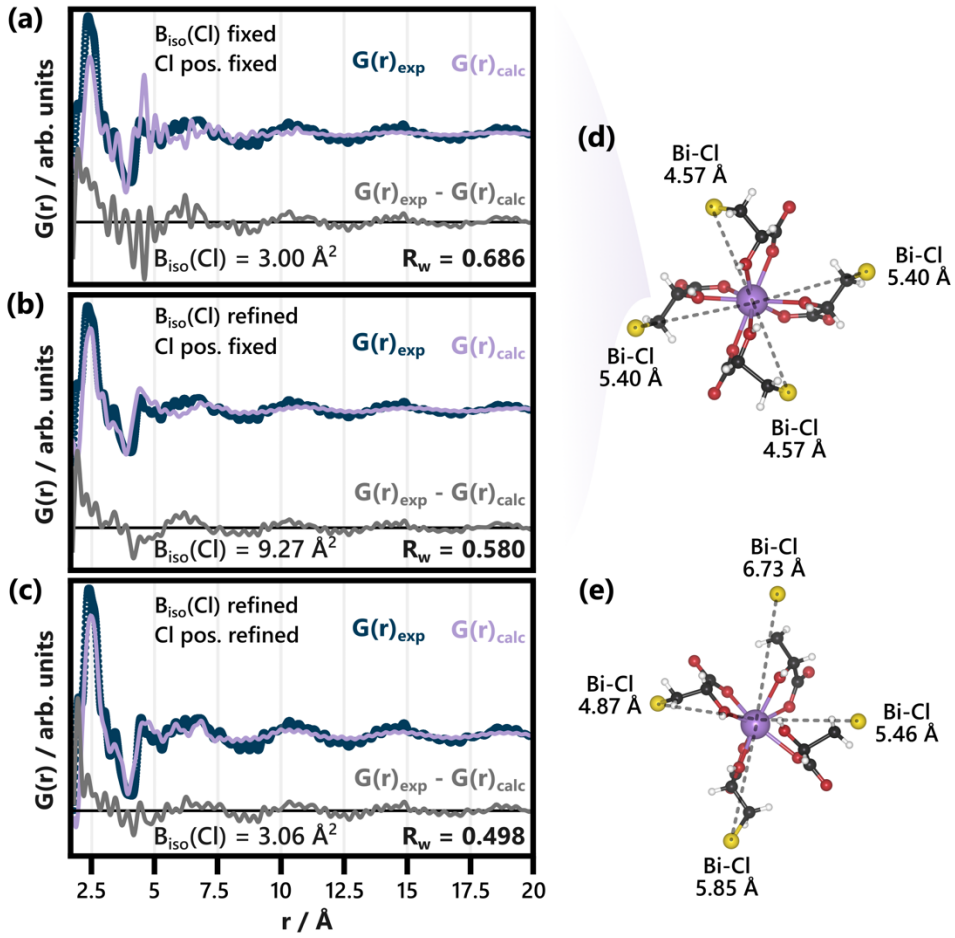

Figure S5. Refinements of the reference complex to the precursor solution PDF obtained through the 'combined background' approach. A fit range from 1.7 to 20 Å was used. The treatment of the chlorine positions varies: (a) Both the position and the atomic displacement parameters (B_{iso}) of the Cl atoms stay fixed. (b) The Cl B_{iso} values were refined while the Cl positions remain fixed. (c) Both positions and B_{iso} values of the Cl atoms are refined. (d) and (e) show the initial reference complex and the one resulting from refined Cl positions respectively, both with highlighted Bi-Cl distances. For the xyz positions corresponding to (d) and (e), see Tables S1 and S3, respectively. All other results of the refinements are listed in Table S2.

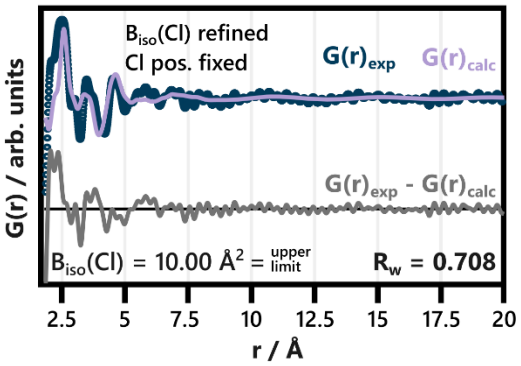

Figure S6. Refinement of the BiClLac complex to the 'combined background' precursor PDF acquired for 10 s. A fit range from 1.7 to 20 Å was used. Analogously to Figure 1d, the Cl B_{iso} values are refined, and the Cl positions are fixed. The results of the refinement are listed in Table S4.

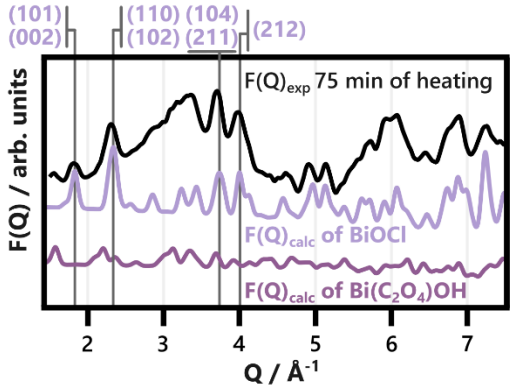

Figure S7. Comparison of the *in situ* F(Q) frame after 75 min of heating with the calculated reference patterns of BiOCl (ICSD code 74502)[5] and $Bi(C_2O_4)OH$ (ICSD code 419313)[6]. To match the low Q resolution obtained in the RA-PDF setup, the theoretical patterns are artificially broadened. Characteristic Bragg peaks belonging to BiOCl are assigned to the lattice planes giving rise to them.

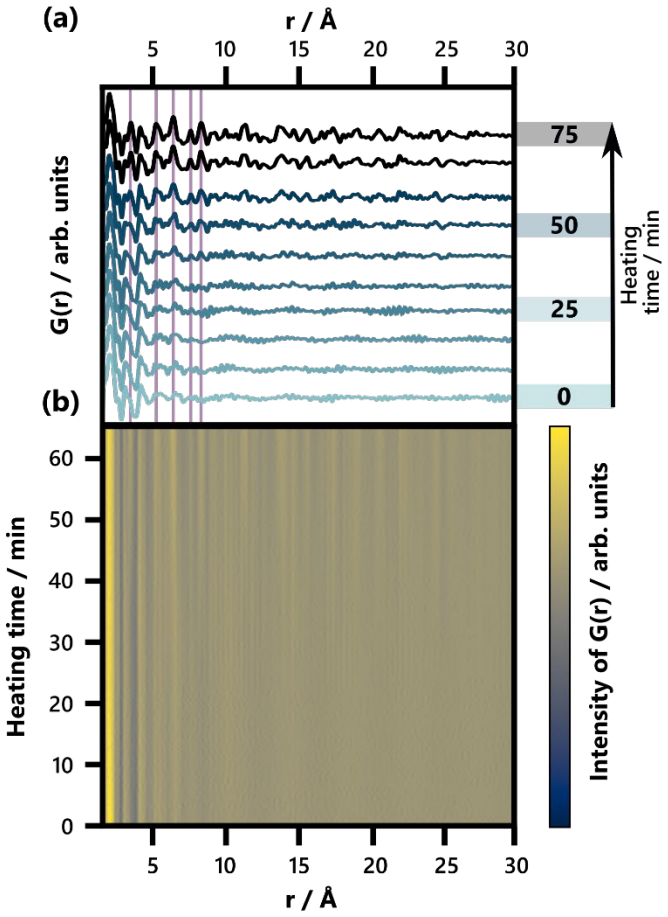

Figure S8. Equivalent plot to Figures 2b and 2e with an r_{max} of 30 Å. (a) Selected G(r) patterns obtained between 0 and 75 min of heating, shown in increments of 8.3 min. Characteristic interatomic distances of BiOCl are highlighted. (b) Full set of time-resolved G(r) patterns with a color scale where yellow and blue represent high and low intensity, respectively.

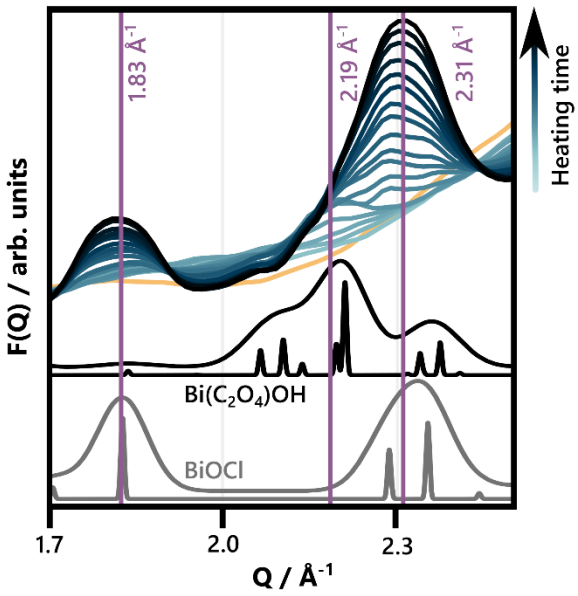

Figure S9. Selected F(Q) patterns obtained between 16.6 and 75 min of heating (going from light to dark blue), shown in increments of 3.3 min. The F(Q) of the unheated precursor solution is given for reference in yellow. Emerging Bragg peaks are highlighted and qualitatively assigned to the two product phases. The two broad peaks observed at 1.83 $Å^{-1}$ and 2.31 $Å^{-1}$ are allocated to their respective lattice planes in Figure S7.

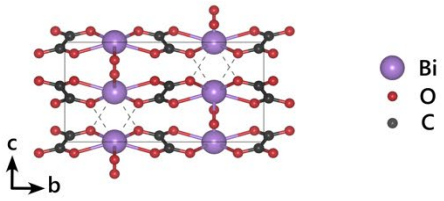

Figure S10. Crystal structure of $Bi(C_2O_4)OH$ (ICSD code 419313)[6] shown along the *a* axis. Bi, O, and C atoms are visualized in purple, red, and black, respectively, whereas the H atoms are omitted for clarity.

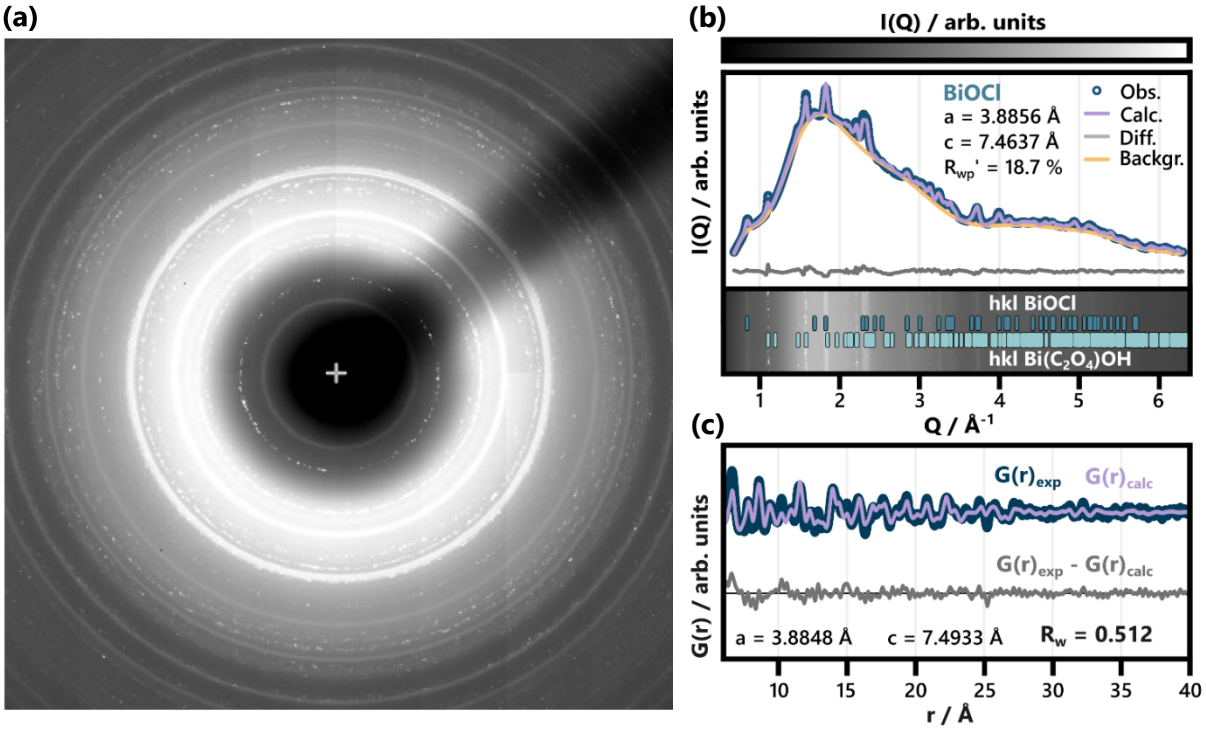

Figure S11. Analysis of (a) the 2D diffraction pattern of the product obtained from a two-step heating experiment. (b) Two-phase Rietveld refinement of BiOCl (ICSD code 74502)[5] and $Bi(C_2O_4)OH$ (ICSD code 419313)[6] to the PXRD pattern of the product phase in solution. The calibrated 1D diffraction pattern is the result of a radial integration of (a) The pattern highlights the *hkl* positions of the two phases and allows for the allocation of the solid and spotty diffraction rings to BiOCl and $Bi(C_2O_4)OH$, respectively. (c) Refinement of BiOCl to the product PDF (110 min heating) of the same experiment as the data shown in (a). A fit range from 6 to 40 Å was used. The results of the Rietveld refinement and the PDF refinement are listed in Tables S6 and S7, respectively.

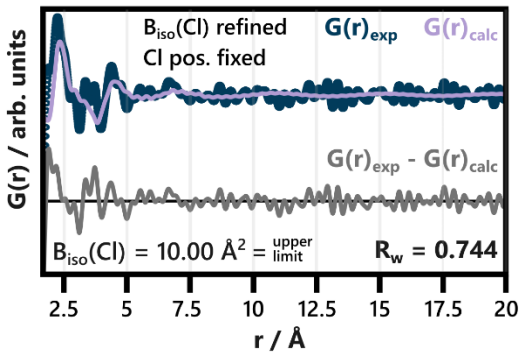

Figure S12. Refinement of the BiClLac complex to the difference curve ($G(r)_{exp,\ 75\ min} - G(r)_{calc}$) of the fit in Figure 3a. A fit range from 1.7 to 20 Å was used. The Cl B_{iso} values are refined, and the Cl positions are fixed. The results of the refinement are listed in Table S8.

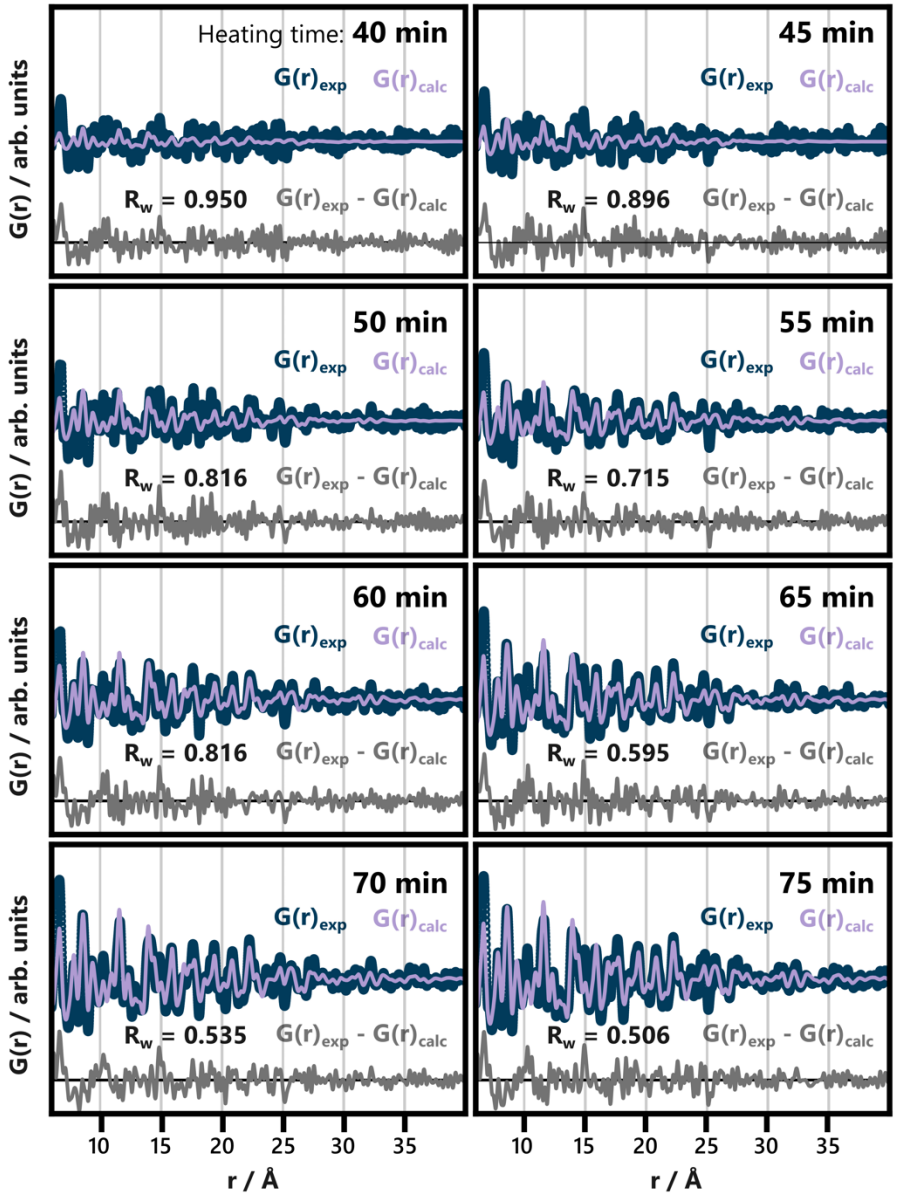

Figure S13. Refinements of BiOCl (ICSD code 74502)[5] to selected frames of the *in situ* PDF data, collected between 40 and 75 min of heating time separated by 5 min each. The individual refinements were conducted with the same refinement parameters as the sequential refinement visualized in Figure 4 and S14, but without Nyquist data sampling. The results of the refinements are listed in Table S10 and S11.

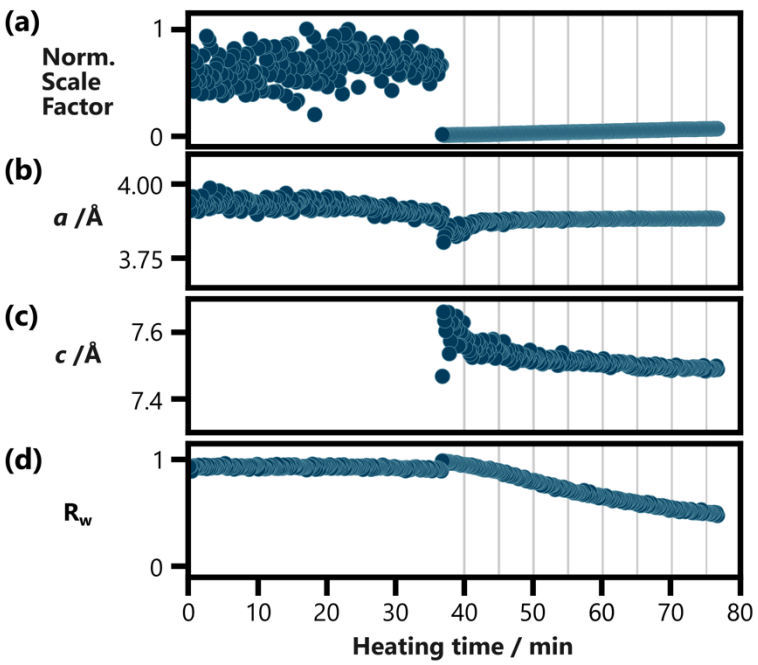

Figure S14. Results of the sequential refinement of BiOCl (ICSD code 74502)[33] to the *in situ* PDF data, as visualized in Figure 4, plotted against time over the whole duration of the experiment. (a) The normalized scaling factor, the lattice parameters (b) *a* and (c) *c*, as well as (d) the fit agreement parameter, R_w, are shown. The spherical particle size was refined as well but was omitted here as it does not carry physical meaning for anisotropic BiOCl particles. Light grey vertical reference lines indicate the times chosen for the individual refinements given in Figure S13. The results obtained for the initial frame of the sequential refinement are listed in Table S9.

Supplemental Tables:

Table S1. List of the xyz coordinates of all atoms in the BiClLac complex reference structure shown in Figure 1a and Figure S5d is comprised of.

Index	Atom	position in x / Å	position in y / Å	position in z / Å
1	Cl	2.755806	4.507717	16.965258
2	Cl	11.946252	4.507717	11.536284
3	O	5.859561	1.919917	14.004707
4	O	8.842497	1.919917	14.496834
5	O	7.552441	3.219057	11.860441
6	O	7.149617	3.219057	16.641100
7	O	5.011173	4.260788	14.834102

8	O	9.690885	4.260788	13.667439
9	H	4.699124	4.946638	14.668793
10	H	10.002934	4.946638	13.832748
11	O	6.906426	5.614059	12.762990
12	O	3.951305	0.896614	14.500824
13	O	10.750753	0.896614	14.000717
14	O	7.741727	3.973434	9.764628
15	O	6.960331	3.973434	18.736914
16	C	7.447031	4.111640	10.999695
17	C	7.255027	4.111640	17.501846
18	C	4.042691	3.227695	14.931768
19	C	10.659367	3.227695	13.569774
20	H	3.253658	3.458212	14.362288
21	H	11.448400	3.458212	14.139254
22	C	4.649602	1.906097	14.448761
23	C	10.052456	1.906097	14.052780
24	C	3.586124	3.034782	16.373184
25	C	11.115934	3.034782	12.128356
26	H	2.969876	2.262070	16.424469
27	H	11.732182	2.262070	12.077072
28	H	4.370471	2.842232	16.945705
29	H	10.331587	2.842232	11.555836
30	Bi	7.351029	3.705141	14.250771
31	C	5.444531	5.630759	10.765982
32	H	5.495045	5.682402	9.777929
33	Cl	4.547864	4.649494	10.760282
34	Cl	10.154194	4.649494	17.741259
35	O	8.003403	5.568566	15.698649
36	C	7.040280	5.620394	11.412017
37	C	7.661778	5.620394	17.089523
38	C	7.465720	4.209537	11.005395
39	C	7.236339	4.209537	17.496145
40	H	6.649014	6.346795	13.113141
41	H	8.216275	6.301740	15.503698
42	H	7.431107	6.185209	10.932469
43	H	7.270951	6.185209	17.569073
44	C	8.897216	5.914082	17.916069
45	H	5.040875	6.471935	11.096315
46	H	5.040875	6.471935	11.096315
47	H	8.638878	5.982414	18.870131

Table S2. Results of refining the BiClLac model structure (Figure 1a) to the PDF of the unheated precursor solution acquired *ex situ* for 10 min and treated with the 'combined background'. A fit range from 1.7 to 20 Å was used. These refinements are shown in Figure S5a, Figure 1d, and Figure S5c. Note, that Figure S5b and Figure 1d show the same fit. All refinements were obtained *via* the DebyePDFCalculator in Diffpy-CMI.[8] The atomic displacement parameters B_{iso} were restricted for both Cl and Bi, to avoid uncontrolled overcompensation of mismatches through the assumption of increased atomic movement. The lower bound (LB) and upper bound (UB) are listed in an additional column ('restr.') for each refinement. The B_{iso} restrictions were loosened for Figure 1d/S5b to follow the extent which the atomic displacement parameters would increase if allowed to. Cl positions that have not been refined are denoted with '/' and remained as listed in Table S1.

Parameter	**Figure S5a**	**Restr.**	**Figure 1d / Figure S5b**	**Restr.**	**Figure S5c**	**Restr.**
R_w	0.686		0.580		0.498	
Bi pos. in x / Å	7.3280		7.2839		7.5510	
Bi pos. in y / Å	3.7635		3.7028		3.5529	
Bi pos. in z / Å	1.3909		1.3881		1.4486	
B_{iso} of Bi / Å^2	2.00	fixed	2.5	LB: 0 UB: 10	5.00	LB: 0 UB: 5
Cl1 pos. in x / Å	/		/		1.8664	
Cl1 pos. in y / Å	/		/		5.9554	
Cl1 pos. in z / Å	/		/		1.7161	
Cl2 pos. in x / Å	/		/		1.2758	
Cl2 pos. in y / Å	/		/		3.8414	
Cl2 pos. in z / Å	/		/		1.1802	
Cl3 pos. in x / Å	/		/		4.3236	
Cl3 pos. in y / Å	/		/		4.9120	
Cl3 pos. in z / Å	/		/		1.0296	
Cl4 pos. in x / Å	/		/		9.6892	
Cl4 pos. in y / Å	/		/		4.4687	
Cl4 pos. in z / Å	/		/		1.8767	
Common B_{iso} for all Cl / Å^2	3.00	fixed	9.31	LB: 0 UB: 10	3.06	LB: 0 UB: 5
Scale	2.56		3.38		4.17	

Table S3. List of the xyz coordinates of all atoms in the BiClLac complex reference structure with refined Cl positions, shown in Figure S5e, is comprised of.

Index	Atom	position in x / Å	position in y / Å	position in z / Å
1	Cl	1.86637	5.95545	17.1609
2	Cl	12.7577	3.84135	11.8022
3	O	5.859561	1.919917	14.004707
4	O	8.842497	1.919917	14.496834
5	O	7.552441	3.219057	11.860441
6	O	7.149617	3.219057	16.641100
7	O	5.011173	4.260788	14.834102
8	O	9.690885	4.260788	13.667439
9	H	4.699124	4.946638	14.668793
10	H	10.002934	4.946638	13.832748
11	O	6.906426	5.614059	12.762990
12	O	3.951305	0.896614	14.500824
13	O	10.750753	0.896614	14.000717
14	O	7.741727	3.973434	9.764628
15	O	6.960331	3.973434	18.736914
16	C	7.447031	4.111640	10.999695
17	C	7.255027	4.111640	17.501846
18	C	4.042691	3.227695	14.931768
19	C	10.659367	3.227695	13.569774
20	H	3.253658	3.458212	14.362288
21	H	11.448400	3.458212	14.139254
22	C	4.649602	1.906097	14.448761
23	C	10.052456	1.906097	14.052780
24	C	3.586124	3.034782	16.373184
25	C	11.115934	3.034782	12.128356
26	H	2.969876	2.262070	16.424469
27	H	11.732182	2.262070	12.077072
28	H	4.370471	2.842232	16.945705
29	H	10.331587	2.842232	11.555836
30	Bi	7.351029	3.705141	14.250771
31	C	5.444531	5.630759	10.765982
32	H	5.495045	5.682402	9.777929
33	Cl	4.323590	4.912000	10.295600
34	Cl	9.689190	4.468740	18.767000
35	O	8.003403	5.568566	15.698649
36	C	7.040280	5.620394	11.412017
37	C	7.661778	5.620394	17.089523

38	C	7.465720	4.209537	11.005395
39	C	7.236339	4.209537	17.496145
40	H	6.649014	6.346795	13.113141
41	H	8.216275	6.301740	15.503698
42	H	7.431107	6.185209	10.932469
43	H	7.270951	6.185209	17.569073
44	C	8.897216	5.914082	17.916069
45	H	5.040875	6.471935	11.096315
46	H	5.040875	6.471935	11.096315
47	H	8.638878	5.982414	18.870131

Table S4. Results of refining the BiClLac model structure (Figure 1a) to the PDF of the unheated precursor solution acquired for 10 s and treated with the 'combined background'. A fit range from 1.7 to 20 Å was used. The refinement is shown in Figure S6 and was obtained *via* the DebyePDFCalculator in Diffpy-CMI.[8] The atomic displacement parameters B_{iso} were restricted for both Cl and Bi, to avoid uncontrolled overcompensation of mismatches through the assumption of increased atomic movement. The lower bound (LB) and upper bound (UB) are listed in an additional column ('restr.').

Parameter	**Figure S6**	**Restr.**
R_w	0.708	
Bi pos. in x / Å	7.5510	
Bi pos. in y / Å	3.5096	
Bi pos. in z / Å	1.4410	
B_{iso} of Bi / Å^2	2.54	LB: 0 UB: 10
Common B_{iso} for all Cl / Å^2	10.00	LB: 0 UB: 10
Scale	6.38	

Table S5. Results of refining the crystal structure of BiOCl (ICSD code 74502)[5] (Figure S1) to the product PDF corresponding to the last frame in Figure 2b (75 min of heating). The refinements are shown in Figure 3 and were obtained *via* real space Rietveld refinements in PDFgui.[9] Note that the spherical diameter parameter does not yield reliable results for anisotropic particles like BiOCl nanoplatelets.

Parameter	**Figure 3a**	**Figure 3b**
Fit range	**2 - 40 Å**	**6 – 40 Å**
R_w	0.854	0.506
a / Å	3.8799	3.8828
c / Å	7.4969	7.4899
Spherical diameter / Å	133.35	60.44
Scale	0.081	0.118

Table S6. Rietveld refinement results of the two-phase refinement on the PXRD data of the product phase in solution, shown in Figure S11b. Apart from the parameters listed below, the scale factors of both phases, the peak shape of BiOCl and peak asymmetry of both phases was refined. We used a polynomial function to model the background caused by solution and glass contributions (shown in yellow in Figure S11b).

Product	**Parameter**	**Result**
	R_{wp}' / %	18.7
BiOCl (ICSD code 74502)[5]		
Unit cell	a / Å	3.8856
	c / Å	7.4637
Preferred orientation	March parameter along (001)	1.2113
$Bi(C_2O_4)OH$ (ICSD code 419313)[6]		
Unit cell	a / Å	6.0726
	b / Å	11.4002
	c / Å	5.9414

Table S7. Results of refining the crystal structure of BiOCl (ICSD code 74502)[5] (Figure S1) to the product PDF corresponding to the acquired PXRD data. The refinement is shown in Figure S11c and was obtained *via* real space Rietveld refinement [9]in PDFgui[9], using a fit range of 6 to 40 Å. Note that the spherical diameter parameter does not yield reliable results for anisotropic particles like BiOCl nanoplatelets.

Parameter	**Figure S11c**
R_w	0.512
a / Å	3.8848
c / Å	7.4933
Spherical diameter / Å	66.36
Scale	0.075

Table S8. Results of refining the BiClLac model structure (Figure 1a) to the difference curve ($G(r)_{exp,\ 75\ min}$ - $G(r)_{calc}$) of the fit in Figure 3a. A fit range from 1.7 to 20 Å was used. The refinement is shown in Figure S12 and was obtained *via* the DebyePDFCalculator in Diffpy-CMI.[8] The atomic displacement parameters B_{iso} were restricted for both Cl and Bi, to avoid uncontrolled overcompensation of mismatches through the assumption of increased atomic movement. The lower bound (LB) and upper bound (UB) are listed in an additional column ('restr.').

Parameter	**Figure S12**	**Restr.**
R_w	0.744	
Bi pos. in x / Å	7.5510	
Bi pos. in y / Å	3.6128	
Bi pos. in z / Å	1.4497	
B_{iso} of Bi / Å^2	9.18	LB: 0 UB: 10
Common B_{iso} for all Cl / Å^2	10.00	LB: 0 UB: 10
Scale	5.95	

Table S9. Results of the initial refinement serving as a starting point for sequentially refining BiOCl (ICSD code 74502)[5] to the *in situ* PDF data. The results obtained for all refinements of the sequence are visualized in Figure 4 and S14 for a selected time range and the whole experiment, respectively. Nyquist data sampling was used for all but the initial frame of the sequential refinement (76.6 min of heating). The real space Rietveld refinements were conducted in PDFgui[9], using a fit range of 6 to 40 Å. Note that the spherical diameter parameter does not yield reliable results for anisotropic particles like BiOCl nanoplatelets.

Parameter	**Initial frame 76.6 min heating**
R_w	0.492
a / Å	3.8835
c / Å	7.4857
Spherical diameter / Å	59.27
Scale	0.122

Table S10. The first half of the results obtained for refining BiOCl (ICSD code 74502)[5] to selected frames of the *in situ* PDF data (Figure S13). Frames collected between 40 and 55 min of heating time separated by 5 min each are covered in this table, for the frames between 60 and 75 min of heating, see Table S11. The individual refinements were conducted with the same refinement parameters as the sequential refinement visualized in Figure 4 and S14, but without Nyquist data sampling. The real space Rietveld refinements were conducted in PDFgui[9], using a fit range from 6 to 40 Å. Note that the spherical diameter parameter does not yield reliable results for anisotropic particles like BiOCl nanoplatelets.
[5]

Parameter	**40 min heating**	**45 min heating**	**50 min heating**	**55 min heating**
R_w	0.950	0.896	0.816	0.715
a / Å	3.8631	3.8691	3.8820	3.8830
c / Å	7.5601	7.5392	7.5122	7.5074
Spherical diameter / Å	51.77	44.96	48.72	55.31
Scale	0.019	0.035	0.051	0.062

Table S11. The second half of the results obtained for refining BiOCl (ICSD code 74502)[5] to selected frames of the *in situ* PDF data (Figure S13). Frames collected between 60 and 75 min of heating time separated by 5 min each are covered in this table, for the frames between 40 and 55 min of heating, see Table S10. The individual refinements were conducted with the same refinement parameters as the sequential refinement visualized in Figure 4 and S14, but without Nyquist data sampling. The real space Rietveld refinements were conducted in PDFgui[9], using a fit range from 6 to 40 Å. Note that the spherical diameter parameter does not yield reliable results for anisotropic particles like BiOCl nanoplatelets.

Parameter	**60 min heating**	**65 min heating**	**70 min heating**	**75 min heating**
R_w	0.652	0.595	0.535	0.506
a / Å	3.8817	3.8844	3.8836	3.8829
c / Å	7.5194	7.4877	7.4896	7.4899
Spherical diameter / Å	58.56	55.81	57.084	60.45
Scale	0.073	0.094	0.108	0.118

Supplemental References:

1. T. Egami and S. J. L. Billinge, *Underneath the Bragg Peaks: Structural Analysis of Complex Materials*, Pergamon, Oxford/Amsterdam/San Diego, 2nd edn., 2012.
2. G. E. Brown and G. V. Gibbs, *Am. Mineral.*, 1969, **54**, 1528-1539.
3. P. J. Chupas, X. Qiu, J. C. Hanson, P. L. Lee, C. P. Grey and S. J. L. Billinge, *J. Appl. Crystallogr.*, 2003, **36**, 1342-1347.
4. B. Ingham, *J. Appl. Crystallogr.*, 2014, **47**, 166-172.
5. K. G. Keramidas, G. P. Voutsas and P. I. Rentzeperis, *Z. Kristallogr.*, 1993, **205**, 35-40.
6. M. Rivenet, P. Roussel and F. Abraham, *J. Solid State Chem.*, 2008, **181**, 2586-2590.
7. G. W. Zack, W. E. Rogers and S. A. Latt, *J. Histochem. Cytochem.*, 1977, **25**, 741-753.
8. P. Juhás, C. L. Farrow, X. Yang, K. R. Knox and S. J. Billinge, *Acta Crystallogr., Sect. A: Found. Adv.*, 2015, **71**, 562-568.
9. C. L. Farrow, P. Juhás, J. W. Liu, D. Bryndin, E. S. Božin, J. Bloch, T. Proffen and S. J. L. Billinge, *J. Phys.: Condens. Matter*, 2007, **19**, 335219.